Strehl ratio and amplitude-weighted generalized orthonormal Zernike-based polynomials

COSMAS MAFUSIRE* AND TJAART P. J. KRÜGER

Department of Physics, Faculty of Natural and Agricultural Science, University of Pretoria, Private Bag X20, Hatfield 0028, South Africa

**Corresponding author: cosmasmafusire@gmail.com*

The concept of orthonormal polynomials is revisited by developing a Zernike-based orthonormal set for a non-circular pupil that is transmitting an aberrated, non-uniform field. We refer to this pupil as a general pupil. The process is achieved by using the QR form of the Gram Schmidt procedure on Zernike circle polynomials and is interpreted as a process of balancing each Zernike circle polynomial by adding those of lower order in the general pupil, a procedure which was previously performed using classical aberrations. We numerically demonstrate this concept by comparing the representation of phase in a square-Gaussian pupil using the Zernike-Gauss square and Zernike-circle polynomials. As expected, using the Strehl ratio, we show that only specific lower-order aberrations can be used to balance specific aberrations, for example, tilt cannot be used to balance spherical aberration. In the process, we present a possible definition of the Maréchal criterion for the analysis of the tolerance of systems with apodized pupils.

OCIS codes: (080.1005) Aberration expansions; (120.5050) Phase measurement; (110.0110) Imaging systems; (000.4430) Numerical approximation and analysis.

1. Introduction

The phase of a weakly aberrated uniform optical field through a circular pupil can be represented by expansion of an infinite discrete set, known as the Zernike circle (ZC) polynomial set [1–5]. The ZC set is the only polynomial set derived by balancing Seidel aberrations that are normalized in a unit circle. For this reason, ZC expansion coefficients are associated with experiencing specific optical effects by the field, and so they were initially applied to the problem of diffraction theory of light beams carrying aberrations [6]. The advantages of exploiting the orthonormality of such polynomials include the following:

(1) Each expansion coefficient is unique in that it is independent of the number of polynomials used in a particular expansion.

(2) Only piston has a non-zero mean; therefore, the mean value of a linear combination of an orthonormal set is the piston coefficient, which defines the mean of the wavefront.

(3) The wavefront variance is calculated from the sum of the squares of the non-piston terms.

(4) Each coefficient, except the piston, represents the minimum variance associated with the aberration and, by extension, represents the standard deviation of the respective aberration term.

The last two statements have implications in the design of systems with circular pupils. In a specific phase expansion, removal of one ZC coefficient results in a lower wavefront error, making the phase less deformed. This is the basis of the operation of adaptive optical systems, whether in large telescope systems or in small-scale microscopy applications. They operate by removing aberrations and taking wavefront error measurements until a selected value is achieved. [7].

It is apparent that the advantages of using orthonormal polynomials are lost if the pupil is no longer circular. The case that has been extensively studied is the one that pertains to modern telescope systems, which utilize non-circular mirrors, specifically annular, elliptical, hexagonal, square, rectangular and binocular shapes [8–14]. Polynomials that are orthogonal to these shapes have been available for at least ten years [8]. They were achieved using methods such as the recursive Gram–Schmidt procedure [8–15] and nonrecursive methods that include the Cholesky decomposition [16] and diffeomorphism [17]. Collectively, this work has shown that it is indeed possible to generate a polynomial basis set orthonormal in a pupil of any shape and thereby restore the advantages of orthonormality. Moreover, these polynomials are derived from the ZC set, meaning that the process creates the same aberrations, but they are normalized in the non-circular pupil. For this reason, they

can be referred to as orthonormal Zernike-based (OZ) polynomials, of which the ZC set is a special case. The whole process can be summarized as follows: ZC polynomials are derived by balancing classical Seidel aberrations by adding lower-order Seidel polynomials to minimize the variance in circular pupils, whereas OZ polynomials are created by balancing ZC polynomials by adding lower-order ZC polynomials to balance them in non-circular pupils. It is a one-to-one relationship that is carried over from Seidel polynomials to any pupil of choice, indicating that for every Seidel spherical aberration term, there is an equivalent ZC spherical aberration term and an OZ spherical aberration term. By extension, it is possible to derive one OZ set from another, for example, by deriving the Zernike annular set from the Zernike elliptical set. It is also possible to determine an OZ set from the Seidel series [4].

However, minimal effort has been spent on non-uniform or *apodized* fields [18–20]. These fields are generally described as having an amplitude in which the energy is concentrated about the beam axis but decreases as one moves to the margins. Practical realization of these systems includes installing an appropriate absorbing filter at the pupil or using laser transmitters. The finite size of the pupil has the effect of truncating the energy of the field; the bigger the pupil, the less the truncation such that if the beam is sufficiently small, the effects of truncation can be ignored. In 1995, Mahajan introduced the Zernike-Gauss circle and Zernike-Gauss annular polynomials and then investigated their use on weakly truncated, weakly aberrated Gaussian pupils with circular and annular shapes, respectively [21]. In this paper, we extend Mahajan's model to the case of non-uniform fields with general non-circular shapes. Our approach is based on diffraction theory to show the necessity of developing an OZ set for the non-uniform fields in any aperture shape, which we collectively refer to as "general pupils." The model is extended to the case of strongly aberrated systems and analyzed by adding different amounts of ZC defocus and tilt, so that the conditions for maximizing the amplitude-weighted Strehl ratio of the system can be investigated.

The paper is organized as follows: the Strehl ratio of a light field in a general pupil is discussed in Section 2, with emphasis on weakly aberrated systems. In Section 3, a generalized polynomial set is derived, and its mathematical properties are described. A relationship between the orthonormal set and ZC polynomials is derived in Section 4 to emphasize the physical meaning of such a set. In Section 5, we investigate Gaussian light fields in square apertures with the conclusion outlined in Section 6. Throughout this paper, bold small and capital letters are, respectively, used to represent column vectors and matrices where t represents transposition.

2. Amplitude-Weighted Strehl Ratio

In this Section, a theory for the derivation of the Strehl ratio in general pupils is outlined. The pupil function for a system with a general pupil may be presented by a pupil function

$$E(\boldsymbol{\rho}) = \begin{cases} A(\boldsymbol{\rho}) \exp\{i\phi(\boldsymbol{\rho})\}, & \text{inside the aperture} \\ 0, & \text{outside the aperture} \end{cases}, \quad \textbf{(1)}$$

where $i = \sqrt{-1}$ and $A(\boldsymbol{\rho})$ and $\phi(\boldsymbol{\rho})$ are the real amplitude and phase of the field, respectively, with $\boldsymbol{\rho} \in \Re^2$ a position vector representing the transverse normalized spatial coordinates of the field in the pupil. The intensity of the focused field in the image plane at a distance R behind the pupil can be calculated through the diffraction equation [4,22]

$$I(\boldsymbol{r}) = \left(\frac{k}{2\pi R}\right)^2 \left| \iint A(\boldsymbol{\rho}) \exp\{i\phi(\boldsymbol{\rho})\} \exp\left\{-\frac{ik\boldsymbol{\rho}\cdot\boldsymbol{r}}{R}\right\} \mathrm{d}^2\boldsymbol{\rho} \right|^2, \quad \textbf{(2)}$$

where $\boldsymbol{r} \in \Re^2$ is a position vector representing the transverse spatial coordinates of the field in the image plane. In the context of imaging, the pupil can be considered to be part of a centered optical system through which monochromatic light exits, as shown in Fig. 1. Behind the exit pupil lies the Gaussian plane of a system at distance R away, such that one can imagine a Gaussian reference sphere passing through the center of the pupil, C, centered at $\boldsymbol{r} = \boldsymbol{0}$ at O on the Gaussian plane. It is also assumed that the image space is of unit refractive index. In this case, aberrations can be defined as a deviation from this reference sphere, and they are embodied in the function $\phi(\boldsymbol{\rho})$ and illustrated by the dotted line, which, incidentally, passes through O as well. The mean curvature of $\phi(\boldsymbol{\rho})$ is represented by the observation sphere also passing through C but centered at X, with a radius of curvature R_x. The observation plane is now defocused from the Gaussian image plane and tilted from the axis, a result of the aberrations in the system. The focal spot generated by Eq. (2) is sometimes referred to as the incoherent point spread function (PSF) of the imaging system and indicates that the weighting provided by the amplitude of the field, the aberration composition at the exit pupil, and the shape all clearly influence the value.

The presence of aberrations in an imaging system changes the position of the focus from that at the Gaussian image point Y. There are two main effects for which most basic imaging systems are designed to control, namely, field curvature and distortion. Field curvature is a result of the imaging system concentrating light on the Gaussian plane along the system axis at the center of the Gaussian reference sphere. Deviation from the Gaussian sphere is along the axis where the resultant focal plane is located in front of or behind Gaussian plane. The position of the new foci can be calculated using [23]:

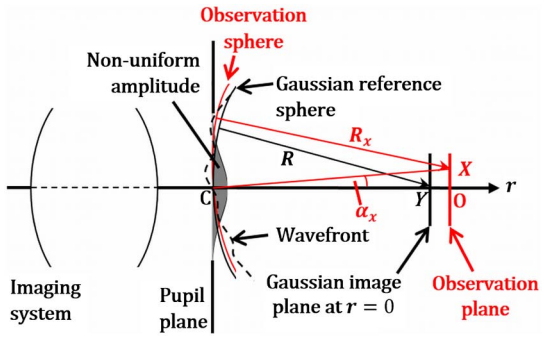

Fig. 1. Schematic diagram of an imaging system focusing non-uniform light on a Gaussian plane at point O. The presence of aberrations results in a new focal point, X, on the defocused observation plane.

$$R_x = -\frac{k\iint x^2 A^2(\boldsymbol{\rho})\mathrm{d}^2\boldsymbol{\rho}}{\iint x\partial_x\phi(\boldsymbol{\rho})A^2(\boldsymbol{\rho})\mathrm{d}^2\boldsymbol{\rho}},$$
$$R_y = -\frac{k\iint y^2 A^2(\boldsymbol{\rho})\mathrm{d}^2\boldsymbol{\rho}}{\iint y\partial_y\phi(\boldsymbol{\rho})A^2(\boldsymbol{\rho})\mathrm{d}^2\boldsymbol{\rho}}. \quad (3)$$

due to the phase $\phi(\boldsymbol{\rho})$, where $\boldsymbol{\rho} = \boldsymbol{\rho}(x, y)$. If the aberration consists only of system field curvature, then both R_x and R_y will reduce to R. Deviation from the Gaussian plane can be corrected by moving the observation plane to the new focal plane, a process called defocusing. Alternatively, distortion alters the direction of the propagation of light such that the centroid of the image spot moves transversely. The centroid coordinates at the image plane, $(\langle x\rangle_i, \langle y\rangle_i)$, result in the beam pointing [4]

$$\alpha_x = \frac{\langle x\rangle_i}{R} = \frac{\iint \partial_x\phi(\boldsymbol{\rho})A^2(\boldsymbol{\rho})\mathrm{d}^2\boldsymbol{\rho}}{\iint A^2(\boldsymbol{\rho})\mathrm{d}^2\boldsymbol{\rho}},$$
$$\alpha_y = \frac{\langle y\rangle_i}{R} = \frac{\iint \partial_y\phi(\boldsymbol{\rho})A^2(\boldsymbol{\rho})\mathrm{d}^2\boldsymbol{\rho}}{\iint A^2(\boldsymbol{\rho})\mathrm{d}^2\boldsymbol{\rho}}. \quad (4)$$

Distortion can be corrected by tilting the image plane by an amount equal to the amount of distortion in the system. Note that for Eqs. (3) and (4), $\phi(\boldsymbol{\rho})$ should be a sum of the amount of field curvature in the system added to the extra phase function due to unwanted aberrations.

It is possible to defocus and tilt the image plane until the best image is acquired. The simplest control parameter is to measure the amount of light delivered to the center of the image plane. This is because the presence of aberrations in the system results in deflection of some of the light from the center of the PSF, the amount of which depends on the strength of the aberrations. This phenomenon is characterized by the Strehl ratio [3,24], which can be expressed as a measure of the performance of an optical system in image formation, and it is defined, in our case, as a ratio of the PSF at $\boldsymbol{r} = \boldsymbol{0}$ with and without aberrations. After making the necessary adjustments, the amplitude-weighted Strehl ratio, S, in the image plane is cast into

$$S = \frac{I_\phi(\boldsymbol{r}=0)}{I_{\phi=0}(\boldsymbol{r}=0)} = \left|\frac{\iint A(\boldsymbol{\rho})\exp\{i\phi(\boldsymbol{\rho})\}\mathrm{d}^2\boldsymbol{\rho}}{\iint A(\boldsymbol{\rho})\mathrm{d}^2\boldsymbol{\rho}}\right|^2$$
$$= |\langle\exp\{i\phi(\boldsymbol{\rho})\}\rangle|^2, \quad (5)$$

also defined as the squared modulus of the amplitude-weighted average of $\exp\{i\phi(\boldsymbol{\rho})\}$ in a general pupil. If the aberrations are small enough, the Strehl ratio can be recast into any one of the forms [4]:

$$S \cong S_1 = 1 - \langle(\Delta\phi(\boldsymbol{\rho}))^2\rangle, \quad \text{Nijboerap proximation},$$
$$S \cong S_2 = \left(1 - \frac{1}{2}\langle(\Delta\phi(\boldsymbol{\rho}))^2\rangle\right)^2, \quad \text{MarOchal approximation},$$
$$S \cong S_3 = \exp\{-\langle(\Delta\phi(\boldsymbol{\rho}))^2\rangle\}, \quad \text{Mahajan approximation}, \quad (6)$$

with S_3 generally considered the most accurate [4]. The term $\langle(\Delta\phi(\boldsymbol{\rho}))^2\rangle$ is the amplitude-weighted wavefront error,

$$\langle(\Delta\phi(\boldsymbol{\rho}))^2\rangle = \langle(\phi(\boldsymbol{\rho}) - \langle\phi(\boldsymbol{\rho})\rangle)^2\rangle, \quad (7)$$

where the angled brackets denote the amplitude-weighted spatial average value of the nth power of the phase,

$$\langle\phi^n(\boldsymbol{\rho})\rangle = \frac{\iint \phi^n(\boldsymbol{\rho})A(\boldsymbol{\rho})\mathrm{d}^2\boldsymbol{\rho}}{\iint A(\boldsymbol{\rho})\mathrm{d}^2\boldsymbol{\rho}}. \quad (8)$$

When $n = 1$ and $n = 2$, Eq. (8) represents the amplitude-weighted mean and the mean of the square of the aberration function, respectively. It is obvious that, in each case, the definition of the Strehl ratio, as defined by Eq. (6), monotonically increases as $\langle(\Delta\phi(\boldsymbol{\rho}))^2\rangle$ is decreased, except for S_2 for large values of the variance. The Maréchal criterion states that a wavefront of a uniform field is regarded as diffraction-limited if its Strehl ratio, $s_2 = (1 - \frac{1}{2}\langle(\Delta\phi_c)^2\rangle)^2 \geq 0.8$, where $\langle(\Delta\phi_c)^2\rangle$ is the variance of a uniform field in a circular pupil. For a given amount of the wavefront variance, the Strehl ratio of a non-uniform pupil is generally higher than that of a uniform pupil [4] by an amount $\Delta S_2 = S_2 - s_2 > 0$. Therefore, the Maréchal criterion for a non-uniform field to be regarded as diffraction-limited is that its Strehl ratio fulfils the following condition, $S_2 = s_2 + \Delta S_2 \geq 0.8 + \Delta S_2$. As a result, the aberration tolerance for a non-uniform pupil is higher than that of a uniform beam for a given Strehl ratio.

3. Zernike-Based Orthonormal Polynomial Set

The purpose of the Zernike-based orthonormal polynomial formulation is to analyze weakly aberrated systems with general pupils by maximizing the Strehl ratio, a condition that is achieved by minimizing the wavefront error. The set needs to meet three additional conditions: it needs to be normalized, linearly independent, and related to classical aberrations. For a unit circle, the ZC set was found to fulfil all three conditions in a circular pupil and so forms the basis for the derivation of the OZ set in general pupil. The ordered OZ set is given by a column vector, $\underline{\boldsymbol{z}}(\boldsymbol{\rho})$, whose elements form the basis in the general pupil, such that the phase can be represented by an expansion

$$\phi(\boldsymbol{\rho}) = \underline{\boldsymbol{c}}^t\underline{\boldsymbol{z}}(\boldsymbol{\rho}), \quad (9)$$

where the column vector $\underline{\boldsymbol{c}}$ contains an ordered set of expansion coefficients. $c^t\boldsymbol{z}(\boldsymbol{\rho})$ is the phase expansion as a sum expressed as an inner product of the two vectors in Euclidean space. It is expected that the OZ set is a complete, orthonormal set which obeys the following equation:

$$\langle\underline{\boldsymbol{z}}(\boldsymbol{\rho})\underline{\boldsymbol{z}}^t(\boldsymbol{\rho})\rangle = \boldsymbol{I}. \quad (10)$$

The matrix on the left-hand side of Eq. (10) is referred to as a Gram matrix [25]. If it is an identity matrix, the implication is that the OZ set is orthonormal with its linear independence being proven by the Gram matrix's non-singularity thereby fulfilling the first two conditions. Therefore, the combination of Eqs. (9) and (10) can be used to generate the expansion coefficient vector

$$\underline{\boldsymbol{c}} = \langle\phi(\boldsymbol{\rho})\underline{\boldsymbol{z}}(\boldsymbol{\rho})\rangle. \quad (11)$$

The average value of the phase can be calculated from Eq. (8) for $n = 1$,

$$\langle\phi(\boldsymbol{\rho})\rangle = \underline{\boldsymbol{c}}^t\boldsymbol{e}_1, \quad (12)$$

where $\boldsymbol{e}_1$ is the first element of the standard basis in an Euclidean plane [25]. In short, the right-hand side in the above equation represents the piston coefficient. The average value of

the phase for $n = 2$ in Eq. (8) is the sum of the square of the coefficients

$$\langle \phi^2(\boldsymbol{\rho}) \rangle = \underline{\boldsymbol{c}}^t \underline{\boldsymbol{c}}. \tag{13}$$

Maximizing the Strehl ratio is achieved by minimizing the wavefront variance, which, incidentally, is given by

$$\langle (\Delta\phi(\boldsymbol{\rho}))^2 \rangle = \underline{\boldsymbol{c}}^t (\boldsymbol{I} - \boldsymbol{e}_1 \boldsymbol{e}_1^t) \underline{\boldsymbol{c}}. \tag{14}$$

4. Derivation of Orthonomal Polynomials from the ZC Set

Having established the mathematical properties of the OZ polynomials, we now proceed to derive a relationship between these polynomials and the ZC set. This way the new set can be related to the classical aberrations, thereby fulfilling the third and last condition to be fulfilled by these polynomials, as mentioned in Section 2. The phase can now be presented as a linear combination of the ZC set:

$$\boldsymbol{z}(\rho, \theta) = \{Z_n^m(\rho, \theta)\}_{j=1}^{\infty} = \{Z_j(\rho, \theta)\}_{j=1}^{\infty}, \tag{15}$$

which form the basis vectors in the circular pupil and where j establishes the ZC set as an ordered set as defined by Noll [2], where $Z_n^m(\rho, \theta) = 0$, when $n - |m|$ is either odd or negative. Thus, the phase function in a circular pupil can be represented as a linear combination of the elements of the set as shown by

$$\phi_c(\rho, \theta) = \boldsymbol{b}^t \boldsymbol{z}(\rho, \theta). \tag{16}$$

The orthonormality and linear independence of the ZC set in a unit circle are verified through the Gram matrix relation, $\frac{1}{\pi}\int_0^{2\pi}\int_0^1 \boldsymbol{z}(\rho, \theta)\boldsymbol{z}^t(\rho, \theta)\rho \mathrm{d}\rho \mathrm{d}\theta = \boldsymbol{I}$. The expansion coefficients can be calculated as elements of a vector equation, $\boldsymbol{b} = \frac{1}{\pi}\int_0^{2\pi}\int_0^1 \phi_c(\rho, \theta)\boldsymbol{z}(\rho, \theta)\rho \mathrm{d}\rho \mathrm{d}\theta$. The first 15 ZC polynomials corresponding to $1 \le j \le 15$ are listed in Table 1.

The QR form of the Gram–Schmidt procedure states that OZ polynomials can be expressed as a linear combination of the ZC set. The procedure then takes the form

Table 1. List of Normalized Zernike Polynomials Up to the Fourth Order

Name of aberration	j	n	m	$Z_j = Z_n^m(\rho,\theta)$
Piston	1	0	0	$Z_1 = 1$
x-Tilt	2	1	1	$Z_2 = 2\rho \cos\theta$
y-Tilt	3	1	−1	$Z_3 = 2\rho \sin\theta$
Defocus	4	2	0	$Z_4 = \sqrt{3}(2\rho^2 - 1)$
y-Astigmatism	5	2	−2	$Z_5 = \sqrt{6}\rho^2 \sin 2\theta$
x-Astigmatism	6	2	2	$Z_6 = \sqrt{6}\rho^2 \cos 2\theta$
y-Coma	7	3	−1	$Z_7 = \sqrt{8}(3\rho^2 - 2)\sin\theta$
x-Coma	8	3	1	$Z_8 = \sqrt{8}(3\rho^2 - 2)\cos\theta$
y-Trefoil	9	3	−3	$Z_9 = \sqrt{8}\rho^3 \sin 3\theta$
x-Trefoil	10	3	3	$Z_{10} = \sqrt{8}\rho^3 \cos 3\theta$
Spherical aberration	11	4	0	$Z_{11} = \sqrt{5}(6\rho^4 - 6\rho^2 + 1)$
x-Secondary astigmatism	12	4	2	$Z_{12} = \sqrt{10}(4\rho^4 - 3\rho^2)\cos 2\theta$
y-Secondary astigmatism	13	4	−2	$Z_{13} = \sqrt{10}(4\rho^4 - 3\rho^2)\sin 2\theta$
x-Quadrafoil	14	4	4	$Z_{14} = \sqrt{10}\rho^4 \cos 4\theta$
y-Quadrafoil	15	4	−4	$Z_{15} = \sqrt{10}\rho^4 \sin 4\theta$

$$\underline{\boldsymbol{z}}(\boldsymbol{\rho}) = \boldsymbol{H}\boldsymbol{z}(\rho, \theta), \tag{17}$$

where $\boldsymbol{H}$ is a lower triangular matrix. Since the elements of vector $\underline{\boldsymbol{z}}(\boldsymbol{\rho})$ are linearly independent, $\boldsymbol{H}$ is nonsingular. $\boldsymbol{H}$ is the transformation matrix associated with change of basis from the circular pupil to the pupil represented by the old basis vector set $\boldsymbol{z}(\rho, \theta)$ to the general pupil represented by the new basis vector set $\underline{\boldsymbol{z}}(\boldsymbol{\rho})$. It helps carry over the properties of the ZC to the OZ set. $\boldsymbol{H}$ can be calculated by eliminating $\underline{\boldsymbol{z}}(\boldsymbol{\rho})$ from Eqs. (10) and (17) and resulting in the following equation:

$$\boldsymbol{H}^t\boldsymbol{H} = \langle \boldsymbol{z}(\rho, \theta)\boldsymbol{z}^t(\rho, \theta) \rangle^{-1}. \tag{18}$$

The matrix on the right-hand side is symmetrical and positive definite, which means that the lower triangular matrix $\boldsymbol{H}$ can be calculated using the Cholesky decomposition [15]. This matrix can be used to relate the expansion coefficients when using either the ZC set or the OZ set to define a general pupil.

The resulting OZ vector is obtained by combining Eqs. (15) and (17):

$$\underline{\boldsymbol{z}}(\boldsymbol{\rho}) = \{\underline{Z}_n^m(\boldsymbol{\rho})\}_{j=1}^{\infty} = \{\underline{Z}_j(\boldsymbol{\rho})\}_{j=1}^{\infty}. \tag{19}$$

Equation (19) indicates that the polynomial sets have a one-to-one relationship. Since $\boldsymbol{H}$ is a lower triangular matrix, Eq. (17) reveals an important property: every term in Eq. (19) is calculated from the respective term in Eq. (15) plus a few of the lower-order terms, a process called balancing. In other words, the ZC set, which is already balanced in the circular pupil, is balanced in the general pupil by adding a number of lower-order ZC terms to generate the OZ polynomials. In a discrete form, Eq. (17) becomes $\underline{Z}_j(\boldsymbol{\rho}) = \sum_{j'=1}^{j} h_{jj'} Z_{j'}(\rho, \theta)$ where $h_{jj'} \in \boldsymbol{H}$. Equation (20) can be written in the form

$$\underline{Z}_j(\boldsymbol{\rho}) = h_{jj}\left(Z_j(\rho, \theta) + \sum_{j'=1}^{j-1} X_{jj'} Z_{j'}(\rho, \theta)\right), \tag{20}$$

where $X_{jj'} = h_{jj'}/h_{jj}$ is the amount of the aberration $Z_{j'}(\rho, \theta)$ added per unit of $Z_j(\rho, \theta)$ to balance $Z_{j'}(\rho, \theta)$, with h_{jj} as a normalizing coefficient.

5. Numerical Results for a Square-Gausian Pupil

It is generally assumed that high power laser sources and diode lasers have square profiles. However, a much more suitable model for such systems is a Gaussian beam going through a square aperture. This represents a prime application for the model developed in this paper, because it represents a non-circular amplitude-weighted pupil. For the choice of the aperture, the unit square inscribed in a unit circle [8] will be represented by the field function

$$E(x, y) = \begin{cases} \exp\{-\gamma^2(x^2 + y^2)\}\exp\{i\phi(x, y)\}, & -\frac{1}{\sqrt{2}} \le x, y \le \frac{1}{\sqrt{2}} \\ 0, & -\frac{1}{\sqrt{2}} > x, y > \frac{1}{\sqrt{2}} \end{cases}, \tag{21}$$

where x and y are normalized at the edge of the circular pupil, which has a radius a. The Gaussian beam truncation ratio is then given by $\gamma = a/\omega$, where ω is the $1/e^2$ beam radius. The larger γ is, the less the truncation and the greater the transmitted energy, leading to stronger apodization. For a square-Gaussian pupil,

the Strehl ratio calculated by substituting Eq. (21) into Eq. (5) is given by

$$S(\gamma) = \left(\frac{\gamma^2}{\pi erf^2(\gamma/\sqrt{2})}\right)^2 \times \left| \int_{-\frac{1}{\sqrt{2}}}^{\frac{1}{\sqrt{2}}} \int_{-\frac{1}{\sqrt{2}}}^{\frac{1}{\sqrt{2}}} \exp\{-\gamma^2(x^2+y^2)\exp\{i\phi(x,y)\}\mathrm{d}x\mathrm{d}y\right|^2. \tag{22}$$

The expansion coefficients of the first 15 square-Gaussian polynomials are shown in Table 2, each for four cases, $\gamma = 0$, 1, 2, and 3. The results for $\gamma = 0$ are for a uniform square pupil and match those introduced in Ref. [8]. The results for the other truncation parameters are introduced in this paper and are presented in the last three columns of Table 2 in numerical form. (We considered the analytical forms too complex to present here.) There is a general trend where the overall value of $h_{jj'}$ increases with γ. It is obvious that each OZ polynomial depends on the same ZC polynomials regardless of the value of γ. For example, OZ spherical aberration depends on the following ZC aberrations: spherical aberration, x- and y-astigmatism, defocus, and piston, but it is independent of x- and y-coma, x- and y-tilt, and x- and y-triangular astigmatism for all γ. In short, each OZ term is built up by adding lower ZC order terms to the ZC term of the same order as the OZ term, all weighted by the appropriate h coefficients. If a particular aberration does not contribute to a specific OZ term, then the respective h becomes 0. An alternative way of investigating this problem is to add an appropriate number of lower-order ZC terms until $S(\gamma)$ is maximized, as we will see in Section 5.B.

A. Strehl Ratio for Zernike-Gauss Square Polynomials

For weakly aberrated systems, the Strehl ratio depends only on aberration variance, regardless of the type of aberration in the system. This is only possible for minimum values of the Strehl

Table 2. Non-Zero Elements of H for the Square-Gaussian Pupil for the Four Truncation Parameters Up to the Fourth Order

						$h_{jj'}$			
$\underline{Z}_j(\rho)$	n	m	$Z_j(\rho,\theta)$	n'	m'	$\gamma = 0$	$\gamma = 1$	$\gamma = 2$	$\gamma = 3$
$\underline{Z}_1$	0	0	Z_1	0	0	1	1	1	1
$\underline{Z}_2$	1	1	Z_2	1	1	$\sqrt{3/2}$	1.31052	1.60774	2.15018
$\underline{Z}_3$	1	−1	Z_3	1	−1	$\sqrt{3/2}$	1.31052	1.60774	2.15018
$\underline{Z}_4$	2	0	Z_4	2	0	$\sqrt{15/2}/2$	1.44567	1.80608	2.79133
			Z_1	0	0	$\sqrt{5/2}/2$	1.04603	1.918	3.78898
$\underline{Z}_5$	2	−2	Z_5	2	−2	$\sqrt{3/2}$	1.40231	2.11052	3.77488
$\underline{Z}_6$	2	2	Z_6	2	2	$\sqrt{15}/2$	2.04448	2.55418	3.94753
$\underline{Z}_7$	3	−1	Z_7	3	−1	$5\sqrt{21/62}/2$	1.59105	2.1764	3.82112
			Z_3	1	−1	$3\sqrt{21/31}/2$	1.61047	3.15016	7.45124
$\underline{Z}_8$	3	1	Z_8	3	1	$5\sqrt{21/62}/2$	1.59105	2.1764	3.82112
			Z_2	1	1	$3\sqrt{21/31}/2$	1.61047	3.15016	7.45124
$\underline{Z}_9$	3	−3	Z_9	3	−3	$\sqrt{155/2}/4$	2.39059	3.30576	6.23033
			Z_7	3	−1	$-13\sqrt{5/62}/4$	−0.8891	−0.755196	−0.448578
			Z_3	1	−1	$-7\sqrt{5/31}/2$	−1.42114	−1.37996	−0.956261
$\underline{Z}_{10}$	3	3	Z_{10}	3	3	$\sqrt{155/2}/4$	2.39059	3.30576	6.23033
			Z_8	3	1	$13\sqrt{5/62}/4$	0.8891	0.755196	0.448578
			Z_2	1	1	$7\sqrt{5/31}/2$	1.42114	1.37996	0.956261
$\underline{Z}_{11}$	4	0	Z_{11}	4	0	$21\sqrt{5/67}/4$	1.57203	2.25669	4.39964
			Z_4	2	0	$25\sqrt{3/67}/4$	1.80653	3.88886	10.4808
			Z_1	0	0	$8/\sqrt{67}$	1.30358	3.03397	9.45089
$\underline{Z}_{12}$	4	2	Z_{12}	4	2	$21\sqrt{5}/16$	3.08155	3.77649	6.01729
			Z_6	2	2	$45\sqrt{3}/16$	5.37606	7.57404	14.7047
$\underline{Z}_{13}$	4	−2	Z_{13}	4	−2	$\sqrt{105}/8$	1.44106	2.18189	4.67145
			Z_5	2	−2	$3\sqrt{7}/8$	1.37632	3.29478	10.7122
$\underline{Z}_{14}$	4	4	Z_{14}	4	4	$3\sqrt{335}/16$	3.6643	4.88242	9.53124
			Z_{11}	4	0	$129\sqrt{5/134}/16$	1.57959	1.60321	1.33506
			Z_4	2	0	$345\sqrt{3/134}/16$	3.35799	3.73743	3.59517
			Z_1	0	0	$261/(8\sqrt{134})$	2.9462	3.37376	3.46106
$\underline{Z}_{15}$	4	−4	Z_{15}	4	−4	$\sqrt{105}/4$	2.88212	4.36378	9.3429

ratio, below which each aberration begins to deviate as the wavefront error increases. In this case, the orthonormal coefficient of each aberration is represented by the standard deviation, $\sqrt{\langle(\Delta\phi_n^m)^2\rangle}$. Figure 2 shows how $S(\gamma)$ varies with OZ x-tilt, defocus, x-astigmatism, x-coma, x-triangular astigmatism, and spherical aberration. The graphs of S_1, S_2, and S_3 are added in each case for comparison. Evidently, $S_1 < S_2 < S_3$ when $\sqrt{\langle(\Delta\phi_n^m)^2\rangle} < 0.25$, and the three approximations are virtually identical for Strehl ratio less than or approximately equal to 0.8 regardless of γ and aperture shape and not just of types of aberrations. However, for strong aberrations, the approximations differ substantially. $S(\gamma)$ was calculated using Eq. (22). The graphs were calculated for the four values of the truncation factor from Table 2 for selected OZ polynomials. In all cases, for each value of $\sqrt{\langle(\Delta\phi_n^m)^2\rangle}$, $s(\gamma)$ increases with increases in γ, with S_3 representing the best approximation.

In the case of $\underline{Z}_1^1$, Fig. 2(a) shows that S_3 slightly overestimates $s(\gamma)$ for the selected values of γ, with increasingly better fit achieved as γ approaches 3. In the cases of $\underline{Z}_2^o$ and $\underline{Z}_2^2$, as seen in Figs. 2(b) and 2(c), respectively, the situation is the opposite in that S_3 underestimates $S(\gamma)$ with the best fit achieved for a uniform field that gets worse as γ increases in size except for $\gamma = 0$ and 1, where S_3 estimates $S(\gamma)$ fairly accurately. However, Figs. 2(d)–2(f) show that S_3 underestimates $S(\gamma)$ for all values of γ with underestimation increasing with decreasing truncation. However, Fig. 2(f) shows that $S(\gamma)$ for $\underline{Z}_4^o$ are fairly close together and, in fact, at the standard deviation of 0.25λ, $S(\gamma)$ approaches the same value of 0.225 at the four values of γ.

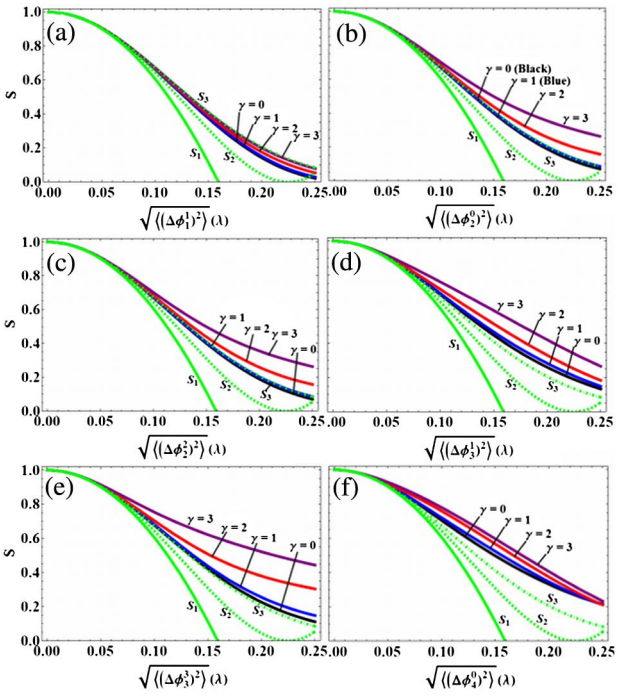

Fig. 2. Dependence of the Strehl ratio on the standard deviation for the aberrations (a) $\underline{Z}_1^1$, (b) $\underline{Z}_2^0$, (c) $\underline{Z}_2^2$, (d) $\underline{Z}_3^1$, (e) $\underline{Z}_3^3$, and (f) $\underline{Z}_4^0$, all in a square-Gaussian pupil. In each graph, S_1, S_2, and S_3 are added for improved perspective.

Figure 2 indicates that both the type of aberration and the truncation ratio appear to be independent of $S(\gamma)$, as expected for near-diffraction-limited systems. The minimum value of $S(\gamma)$ for which the independence can be achieved is different for different aberrations and values of γ. As explained in Section 2, S_2 can be expressed in terms of the Maréchal criterion as having a minimum value of $0.8 + \Delta S_2$. For non-uniform and, for that matter, non-circular uniform pupils, the minimum $S(\gamma)$ is greater than or equal to this value, depending on γ. Here, we present numerical results for ΔS_2 to show that optical systems with general pupils have a lower tolerance compared to those with circular pupils. A method we propose in this paper involves going back to the Maréchal criterion. As mentioned in Section 2, this criterion was devised for circular pupils in which a minimum Strehl ratio of 0.8 is set, which corresponds to a standard deviation of $\lambda/14$. This standard deviation is selected as a maximum for any pupil from which the corresponding minimum Strehl ratio is calculated. The $S(\gamma)$ corresponding to $\sqrt{\langle(\Delta\phi_n^m)^2\rangle} < \lambda/14$ can be read from Fig. 2. It follows that $S_1 = 0.79858$, $S_2 = 0.808722$, and $S_3 = 0.817569$. The corresponding values for $S(\gamma)$ for the square-Gaussian pupils are listed in Table 3. The results show a clear trend in which $S(\gamma)$ increases with γ, an indication that truncation decreases as a result of the optical system having lower tolerance.

B. Strehl Ratio for ZC Aberrations in a Square-Gaussian Pupil

The efficacy of using ZC polynomials in general pupils is now illustrated, using Eq. (22) for specific amounts of selected ZC aberrations and varying amounts of a lower-order aberration. In principle, which aberration combinations lead to a maximum $S(\gamma)$ needs to be determined, particularly for cases where the aberrations are strong. This implies that this is not an attempt to just use the numerical results to derive OZ polynomials but rather to evaluate the extent to which these polynomials can be used in strong aberration regimes. The results from the following numerical model can assist in determining which aberration can be added to a system to control the effects of aberrations already in the system, but it does not provide a method to execute. In short, it is necessary to know which optical effects are associated with which aberrations.

To determine the effects, Eqs. (3) and (4) are used where phase is defined as $\phi = \phi_{sys} + \phi_{ext}$. The system generates a phase of value ϕ_{sys} to the light beam such that it generates the system field curvature $R_x = R_y = R$ if $\phi_{ext} = 0$ is entered into Eq. (3) and centroid values of $\langle x\rangle_i = \langle y\rangle_i = 0$ if entered into Eq. (4). The extra phase term ϕ_{ext} represents

Table 3. Maréchal Criterion Shows the Tolerances of an Imaging System with Square-Gaussian Pupils for the Selected Aberrations Presented, $S(\gamma)$, Corresponding to a Standard Deviation of $\lambda/14$

γ	$\underline{Z}_1^1$	$\underline{Z}_2^0$	$\underline{Z}_2^2$	$\underline{Z}_3^1$	$\underline{Z}_3^3$	$\underline{Z}_4^0$
0	0.8141	0.8164	0.8164	0.8216	0.8185	0.8278
1	0.8145	0.8170	0.8170	0.8242	0.8199	0.8339
2	0.8158	0.8198	0.8198	0.8334	0.8269	0.8556
3	0.8171	0.8263	0.8262	0.8530	0.8458	0.8701

the aberrations from the sample or subject being imaged and generated along the path of the beam as it is transferred from the subject to the entrance pupil. By definition, the size of ϕ_{ext} is beyond the control of the imaging system, at least not directly; indirectly, impact on the imaging process can be minimized by adjusting the observation plane accordingly. In that case, ϕ results in R_x and R_y not necessarily equal to R and nonzero $\langle x \rangle_i$ and/or $\langle y \rangle_i$. This state of affairs is resolved by moving the observation plane longitudinally away from the Gaussian plane, which is called defocusing, and tilting the observation plane, to compensate for the respective changes in field curvature and distortion.

Substituting ϕ as defined by $\phi_{\text{sys}} + \phi_{\text{ext}}$ into Eqs. (3) and (4) can be used to determine whether field curvature and distortion is due to ϕ_{ext}. Let us assume that ϕ_{ext} is due to each aberration listed in Table 1. If ϕ is inserted into Eqs. (3) and (4), then it is now possible to classify each aberration as field curvature/defocus, distortion/tilt, or neither. The result of this exercise is given in Table 4 where Z_2^0, Z_2^2, Z_4^0, Z_4^2, and Z_4^4 focus the field. The astigmatic aberrations Z_2^2 and Z_4^2 also focus the field positively in the x-axis and negatively in the y-axis and vice-versa. For this reason, these two cannot be balanced by defocusing and tilting as discussed so far, but balancing them will be discussed later. In the second column, the aberrations Z_1^1, Z_1^{-1}, Z_3^{-1}, Z_3^1, Z_3^{-3} and Z_3^3 can all alter the pointing of a light beam. The third column contains all aberrations that do not have either effect on a beam, and those effects are outside the scope of this paper.

The phase distribution to be investigated is of the form $\phi_{\text{ext}}(x, y) = C_4^0 Z_4^0(x, y) + C_2^0 Z_2^0(x, y)$, where each coefficient $C_n^m \in \boldsymbol{c}$. The challenge is to establish how much C_2^0 should be added to the system for a fixed amount of C_4^0 associated with the unwanted field curvature to maximize $S(\gamma)$. The phase function can then be recast into the form,

$$\phi_{\text{ext}}(x, y) = C_4^0 \left(Z_4^0(x, y) + \frac{C_2^0}{C_4^0} Z_2^0(x, y) \right). \qquad \textbf{(23)}$$

Figure 3 shows $S(\gamma)$ for selected values of C_4^0 between 0 and 0.5λ in steps of 0.125λ, with each balanced by varying amounts of C_2^0. As expected, increasing the amount of C_4^0 when $C_2^0 = 0$ results in a drop in $S(\gamma)$ for all values of γ, as observed along the vertical axis. The reason for this is that positive C_4^0 pushes the focal plane away from the pupil plane, thereby delivering less light to the center of the image in the observation plane, effectively lowering $S(\gamma)$. This situation can be resolved by moving the observation plane to the new focal plane. The larger C_4^0 is, the greater the amount of C_2^0 required for compensation. In the case of negative C_4^0, the moment of the focal plane is toward the pupil requiring negative defocus to compensate for the movement.

Table 4. Classification of Aberrations According to Effects on the Image Plane

Field curvature/Defocus	Distortion/Tilt	Otherwise
Z_2^0, Z_2^2, Z_4^0, Z_4^2, Z_4^4	Z_1^1, Z_1^{-1}, Z_3^{-1}, Z_3^1, Z_3^{-3}, Z_3^3	Z_2^{-2}, Z_4^{-2}, Z_4^{-4}

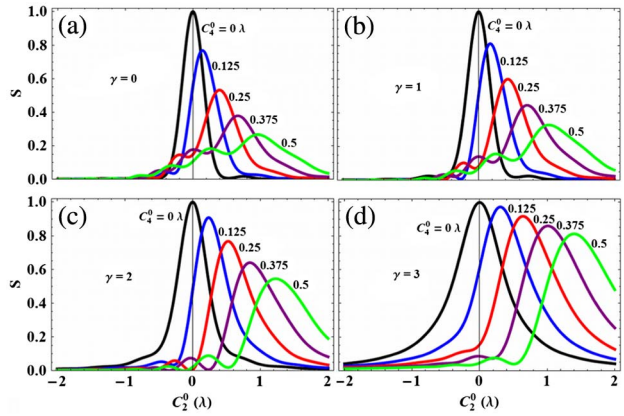

Fig. 3. Maximizing $S(\gamma)$ for systems with C_4^0 by adding varying C_2^0 for γ, equal to (a) 0, (b) 1, (c) 2, and (d) 3.

As Fig. 3 shows, the effect of defocusing the system results in an increase in $S(\gamma)$. The increase in C_4^0 means that maximum $S(\gamma)$ is achieved when using larger C_2^0, though the maximum $S(\gamma)$ actually decreases. A summary of the results is shown in Table 5. Included in this table are results from the theoretical model for weak Z_4^0, where $X_{11,4} = h_{11,4}/h_{11,11}$ takes the values 0.922, 1.187, 1.723, and 2.382 for the γ values 0, 1, 2, and 3, respectively. Values of C_2^0 added to maximize $S(\gamma)$ for each of the investigated values of C_4^0 are shown, and the last set is of the ratio C_2^0/C_4^0, which can be compared with $X_{11,4}$. The results for C_2^0/C_4^0 that come close to the low aberration model of Table 3 are those for which $S(\gamma)$ is above 0.8; in fact, the higher $S(\gamma)$ is, the closer to $X_{11,4}$ the result is, which indicates that the system is approaching the weak aberration conditions. Note that in the case of negative C_4^0, the graphs would mirror those shown in Fig. 3 about the $C_2^0 = 0$ axis.

Next, optical systems with varying amounts of x-coma-induced distortion were investigated. For these systems, C_1^1 can be used to increase $S(\gamma)$, using the following phase function:

$$\phi_{\text{ext}}(x, y) = C_3^1 \left(Z_3^1(x, y) + \frac{C_1^1}{C_3^1} Z_1^1(x, y) \right). \qquad \textbf{(24)}$$

The effect of having this kind of distortion is that, instead of shifting the image longitudinally like for C_4^0, the image is shifted transversely. Positive C_1^1 has the effect of shifting the center of the image in the positive x-direction, which implies that positive C_1^1 is required to move the observation plane by the same amount to compensate. Negative C_3^1 and negative C_1^1 should behave similarly but with a shift in the negative x-direction.

Table 5. Values C_2^0/C_4^0 for Maximum $S(\gamma)$ for $\gamma = 0, 1, 2,$ and 3

		C_2^0/C_4^0 for Maximum $S(\gamma)$			
γ	$X_{11,4}$	0.125	0.250	0.375	0.500
0	0.922	1.200	1.600	1.760	1.800
1	1.149	1.440	1.680	1.920	2.040
2	1.723	1.800	2.160	2.240	2.400
3	2.382	2.400	2.520	2.667	2.760

The numerical results are shown in Fig. 4. As expected, $S(\gamma)$ for $\phi_{\text{ext}}(x,y) = C_3^1 Z_3^1(x,y)$ drops below 1 as soon as C_3^1 becomes finite and continues to drop as C_3^1 increases. However, addition of a sufficient C_1^1 raises $S(\gamma)$, as was observed for spherical aberration. Once again, the maximum $S(\gamma)$ drops with increase in C_3^1. The numerical results for C_3^1 confirm this observation, though the value C_1^1/C_3^1 is shown to increase with increase in C_3^1, as was observed with C_4^0 and C_2^0. The results, in this case, are summarized in Table 6, which also show that the results closest to $X_{8,2}$ are those for which $S(\gamma)$ approaches 1.

For completeness, we now investigate the case of adding an aberration to a system that is already aberrated. The additional aberration will not increase $S(\gamma)$ but rather causes it to drop immediately. We illustrate this using C_1^1 for increasing S of a system with spherical aberration, as shown in Fig. 5. For a uniform field, $\gamma = 0$ [in Fig. 5(a)] and the maximum $S(\gamma)$ is achieved when $C_1^1 = 0$ for all amounts of C_4^0, meaning that any transverse movement of the observation plane results in an automatic drop in light transmitted to the center of the observation plane. An exception emerges, as observed in Figs. 5(b)–5(d), when $C_4^0 = 0.25$, in which case, $S(\gamma)$ is very low, just less than 0.1. These results indicate that it is possible to tilt the observation plane of the system to increase $S(\gamma)$ on systems with unwanted field curvature. However, this is only possible in rare circumstances, and the increase in $S(\gamma)$ achieved is generally very small, in this case the largest achieved is about 0.16 for $\gamma = 3$ indicating the relative uselessness of using tilt to correct for systems with spherical aberration.

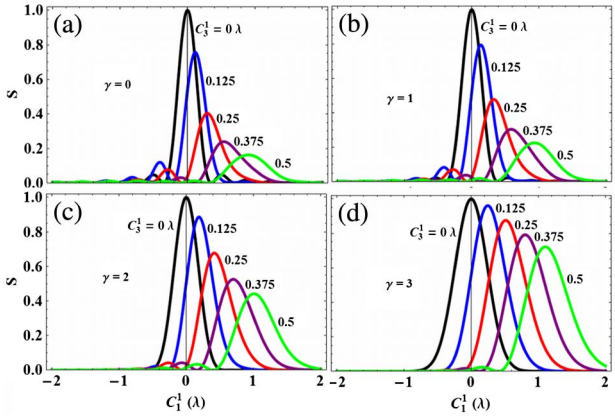

Fig. 4. Maximizing $S(\gamma)$ for systems with fixed C_3^1 by adding varying C_1^1 for γ, equal to (a) 0, (b) 1, (c) 2, and (d) 3.

Table 6. Values of C_1^1/C_3^1 for Maximum $S(\gamma)$ for γ Equal to 0, 1, 2, and 3

		C_1^1/C_3^1 for Maximum $S(\gamma)$			
γ	$X_{8,2}$	0.125	0.250	0.375	0.500
0	0.849	0.800	1.120	1.413	1.800
1	1.012	0.960	1.360	1.573	1.900
2	1.447	1.440	1.600	1.867	2.000
3	1.950	2.000	2.000	2.400	2.200

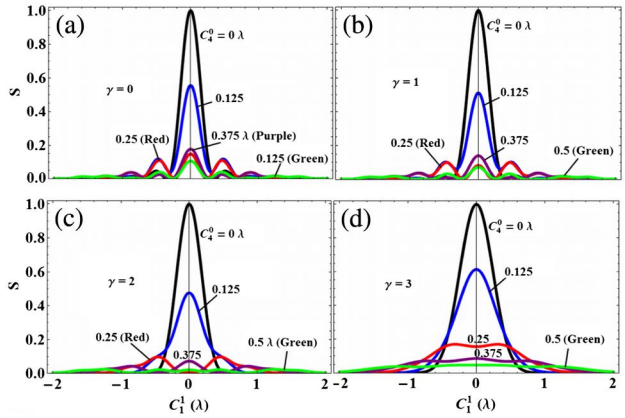

Fig. 5. Maximizing $S(\gamma)$ for systems with fixed C_4^0 by adding varying C_1^1 for γ, equal to (a) 0, (b) 1, (c) 2, and (d) 3.

An interesting problem concerns ZC x-astigmatism, $Z_2^2(x,y)$, which, according to Table 2, does not require addition of any other ZC aberrations to increase $S(\gamma)$. However, inspection of Table 4 tells us that when $\phi_{\text{ext}}(x,y) = C_2^2 Z_2^2(x,y) = \sqrt{6} C_2^2 (x^2 - y^2)$, field curvature would increase in the x-axis and decrease in the y-axis and vice-versa, depending on whether C_2^2 is positive or negative. The independence of the two foci means that it is possible to increase $S(\gamma)$ by using a cylindrical lens. The extra phase in this case is given by $\phi_{\text{ext}}(x,y) = C_2^2 Z_2^2(x,y) + C_{2,x}^0 Z_2^0(x)$, where the extra term actually represents a one-dimensional Zernike defocus in the x-plane, $Z_2^0(x) = \sqrt{3}(2x^2 - 1)$. Adding various amounts of $C_{2,x}^0$ increases $S(\gamma)$, which is not possible to achieve with ZC defocus. The numerical results in Fig. 6 illustrate the outcome, which shows that for all γ, an increasingly negative $C_{2,x}^0$ results in an increase in $S(\gamma)$, leading to a maximum. As was observed with spherical aberration in Fig. 3 and with x-coma in Fig. 4, the maximum achieved $S(\gamma)$ decreases with increasing C_2^2.

The effect of $Z_2^2(x,y)$ can be completely removed from the system if y-defocus, $Z_2^0(y) = \sqrt{3}(2y^2 - 1)$, is also added. The aberration function then becomes $\phi_{\text{ext}}(x,y) = C_2^2 Z_2^2(x,y) + C_{2,x}^0 Z_2^0(x) + C_{2,y}^0 Z_2^0(y)$, which can be simplified using the identity $\sqrt{2} Z_2^2(x,y) \equiv Z_2^0(x) - Z_2^0(y)$ to become

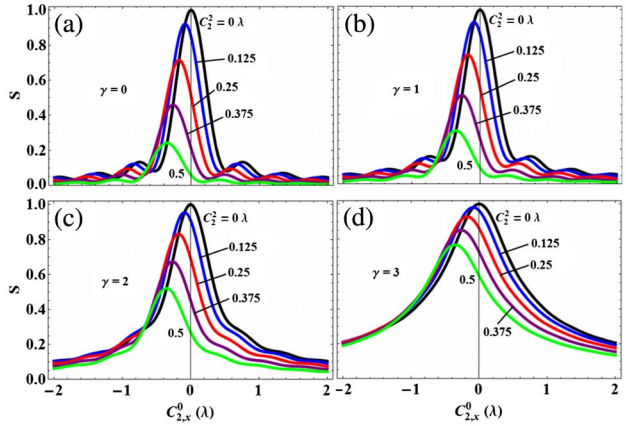

Fig. 6. Maximizing $S(\gamma)$ for systems with fixed C_2^2 by adding varying $C_{2,x}^0$ for γ, equal to (a) 0, (b) 1, (c) 2, and (d) 3.

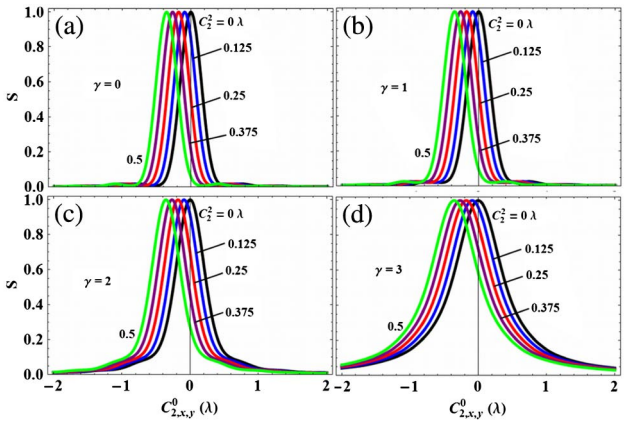

Fig. 7. Maximizing $S(\gamma)$ for systems with fixed C_2^2 by adding varying $C_{2,x,y}^0$ for γ, equal to (a) 0, (b) 1, (c) 2, and (d) 3.

$$\phi_{\text{ext}}(x,y) = \frac{1}{\sqrt{2}} C_2^2 \{Z_2^0(x) - Z_2^0(y)\} + C_{2,x}^0 Z_2^0(x) + C_{2,y}^0 Z_2^0(y). \tag{25}$$

If $C_{2,y}^0 = -C_{2,x}^0 = C_{2,x,y}^0$ is selected, this implies that $\phi_{\text{ext}}(x,y) = 0$ when

$$C_{2,x,y}^0 = -\frac{1}{\sqrt{2}} C_2^2. \tag{26}$$

Folding the observation plane along the x-axis and in the opposite sense along the y-axis with the axes perpendicular and independant of each other creates a toric-shaped plane. Using such an observation plane to conjugate the two field curvatures completely compensates for the x-astigmatism, leading to $S(\gamma) = 1$ as shown in Fig. 7. Note that the value of $C_{2,x,y}^0$ for which $S(\gamma)$ is maximized is the same for all graphs and can be calculated from Eq. (26). An easier alternative would be to insert a toric lens between the pupil and the planar image plane. This is a lens with different optical power and focal length in two orientations perpendicular to each other. This explains why toric lenses are used by ophthamologists to treat patients with astigmatism [26].

6. Conclusions

ZC polynomials have been the standard in wavefront analysis since they were introduced in 1932, and the main limitation is that they are only orthonormal in circular pupils. This has been overcome in the last four decades with the development of other Zernike-based polynomial sets that are orthonormal in noncircular pupils for use in ground-based astronomical systems, which was achieved using the Gram–Schmidt procedure. An important advance was the introduction of the Cholesky decomposition, which is computationally cheaper and less error-prone. The purpose of this paper was to contribute to this progress by investigating imaging systems that use customized light beams as long as the appropriate inner product can be found.

This paper emphasizes the importance of linear algebra to wavefront analysis where an optical pupil is presented as a vector space and the OZ set constitutes the basis vectors. The core of the model is the Gram matrix, which is used to define orthonormality when this matrix is an identity matrix and to define linear independence if it is nonsingular. This approach could be used to normalize any polynomial set, and it has been applied, with great success, in a recently submitted paper in which orthonormal vector polynomials in general pupils were derived by normalizing the Cartesian gradient of the ZC set [27].

The model was then used to generate a Zernike-based polynomial set orthonormal in square-Gaussian pupils, which serves as a possible theoretical representation of the pupil of a diode or high powered laser source. The numerical calculation of the Strehl ratio confirmed that only specific ZC aberrations of a lower order can be used to balance a selected ZC aberration in such a way that addition maximizes the Strehl ratio. Those which do not contribute result in an immediate drop in this parameter. A good example is how, in a square-Gaussian pupils, ZC defocus increases the Strehl ratio in an optical system with ZC spherical aberration but ZC tilt does not. This process demonstrates that calculating the Strehl ratio can be used to numerically derive OZ polynomials, in addition to the Gram–Schmidt procedure.

The aberrations used to balance the selected aberrations can be associated with specific effects, namely, defocus, and tilt. This means that it is possible to design an experiment with an appropriate diffraction optical element or using a spatial light modulator to generate specific ZC aberration and then maximize the Strehl ratio by defocusing the imaging plane by an amount that can be easily measured. This amount of defocus can be related to the spherical aberration, as predicted by the numerical results. The same result is expected using ZC x-tilt to balance ZC x-coma, in which the imaging plane can be tilted by an angle that can also be measured in the lab. This implies that the numerical model discussed in this paper can be used to design an experiment to measure OZ expansion coefficients, a concept which is a subject of future research.

Finally, a method to determine the Maréchal criterion for the analysis of apodized systems is proposed. We assert that for any pupil the wavefront standard deviation maximum should be fixed at $\lambda/14$, but the tolerance be the corresponding Strehl ratio allowed to change with aperture shape and apodization. Our results show that the Strehl ratio for apodized pupils is greater than 0.8, with the value increasing with increased apodization thereby implying a decrease in tolerance.

The work presented here can be applied to the analysis of aberrated light beams, in particular, in settings where the beam quality requires improvement. This would be important for laser-based free space optical communication systems and fiber communication systems. The model presented is also useful for developing more efficient Zernike-based methods to control aberrations in laser-based adaptive optics methods in microscopy and optical communication systems. In addition, imaging systems that use laser radiation, such as super-resolution imaging, are now being augmented by using adaptive systems [28]. For all these cases, adaptive compensation has been the tool of choice, though ZC polynomials are used. It is the intention of the authors of this paper to promote the use of OZ polynomials through the presented numerical results.

References

1. F. Zernike, "Diffraction theory of knife-edge test and its improved form, the phase contrast method," Mon. Not. R. Astron. Soc. **94**, 377–384 (1934).
2. R. J. Noll, "Zernike polynomials and atmospheric turbulence," J. Opt. Soc. Am. **66**, 207–211 (1976).
3. M. Born and E. Wolf, *Principles of Optics: Electromagnetic Theory of Propagation, Interference and Diffraction of Light*, 7th ed. (Cambridge University, 1999).
4. V. N. Mahajan, *Optical Imaging and Aberrations, Part II: Wave Diffraction Optics*, 2nd ed. (SPIE, 2011).
5. V. Lakshminarayanan and A. Fleck, "Zernike polynomials: a guide," J. Mod. Opt. **58**, 1678 (2011).
6. B. R. A. Nijboer, "The diffraction theory of aberrations," Ph. D. Thesis (University of Groningen, 1942).
7. R. K. Tyson, *Principles of Adaptive Optics* 3rd ed. (CRC Press, 2011).
8. V. N. Mahajan and G.-M. Dai, "Orthonormal polynomials in wavefront analysis: analytical solution," J. Opt. Soc. Am. A **24**, 2994 (2007).
9. V. N. Mahajan, "Zernike annular polynomials and optical aberrations of annular pupils," Appl. Opt. **33**, 8125–8127 (1994).
10. W. Swanter and W. W. Chow, "Gram–Schmidt orthonormalization of Zernike polynomials for general aperture shapes," Appl. Opt. **33**, 1832–1937 (1994).
11. R. Upton and B. Ellerbroek, "Gram–Schmidt orthonormalization of the Zernike polynomials on apertures of arbitrary shape," Opt. Lett. **29**, 2840–2842 (2004).
12. V. Mahajan and G.-M. Dai, "Orthonormal polynomials for hexagonal pupils," Opt. Lett. **31**, 2462–2465 (2006).
13. H. Lee, "Use of Zernike polynomials for efficient estimation of orthonormal aberration coefficients over variable noncircular pupils," Opt. Lett. **35**, 2125–2173 (2010).
14. R. J. Mathar, "Orthogonal set of basis functions over the binocular pupil," arXiv:0706.3682 [physics.optics], 2008.
15. D. Watkins, *Fundamentals of Matrix Computations* (Wiley, 2002).
16. G.-M. Dai and V. Mahajan, "Nonrecursive determination of orthonormal polynomials with matrix formulation," Opt. Lett. **32**, 74–76 (2007).
17. R. Navarro, J. L. Lopez, J. A. Diaz, and E. P. Sinusia, "Generalization of Zernike polynomials for regular portions of circles and ellipses," Opt. Express **22**, 21263 (2014).
18. J. Schwiegerling, "Gaussian weighting of ocular wave-front measurements," J. Opt Soc. Am. A **21**, 2065–2072 (2004).
19. J. Nam and J. Rubinstein, "Weighted Zernike expansion with applications to the optical aberration of the human eye," J. Opt. Soc. Am. A **22**, 1709–1716 (2005).
20. K. Liao, Y. Hong, and W. Sheng, "Wavefront aberrations of x-ray dynamical diffraction beams," Appl. Opt. **53**, 6362–6370 (2014).
21. V. Mahajan, "Zernike–Gauss polynomials and aberrations of systems with Gaussian pupils," Appl. Opt. **34**, 8057–8059 (1995).
22. J. W. Goodman, *Introduction to Fourier Optics*, 3rd ed. (Roberts & Company, 2004).
23. C. Mafusire and A. Forbes, "Mean focal length of an aberrated lens," J. Opt. Soc. Am. A **28**, 1403–1409 (2011).
24. V. N. Mahajan, "Strehl ratio of a Gaussian beam," J. Opt. Soc. Am. A **22**, 1824–1833 (2005).
25. J. T. Scheick, *Linear Algebra with Applications* (McGraw-Hill, 1997).
26. H. Momeni-Moghaddam, S. A. Naroo, F. Askarizadeh, and F. Tahmasebi, "Comparison of fitting stability of the different soft toric contact lenses," Contact Lens & Anterior Eye **37**, 346–350 (2014).
27. C. Mafusire and T. P. J. Krüger, "Orthonormal vector polynomials in general pupils," J. Opt. (Manuscript under review).
28. M. Booth, D. Andrade, D. Burke, B. Patton, and M. Zurauskas, "Aberrations and adaptive optics in super-resolution microscopy," Microscopy **64**, 252–261 (2015).